Kaifeng Wang[1]
Key Laboratory of Mechanism Theory and Equipment Design of Ministry of Education, Tianjin University, Tianjin 300354, China;
Department of Industrial and Manufacturing Engineering, Pennsylvania State University, University Park, PA 16802
e-mail: wangkaifeng1987@gmail.com

Piyush Upadhyay[1]
Pacific Northwest National Laboratory, Energy Materials and Manufacturing, Richland, WA 99354
e-mail: Piyush.Upadhyay@pnnl.gov

Yuxiang Wang
Department of Industrial and Manufacturing Engineering, Pennsylvania State University, University Park, PA 16802
e-mail: yww5167@psu.edu

Jingjing Li
Mem. ASME
Department of Industrial and Manufacturing Engineering, Pennsylvania State University, University Park, PA 16802
e-mail: jul572@engr.psu.edu

Xin Sun
Oak Ridge National Laboratory, Energy and Transportation Science Division, Oak Ridge, TN 37932
e-mail: sunx1@ornl.gov

Timothy Roosendaal
Pacific Northwest National Laboratory, Energy Materials and Manufacturing, Richland, WA 99354
e-mail: Timothy.Roosendaal@pnnl.gov

Investigation of Interfacial Layer for Friction Stir Scribe Welded Aluminum to Steel Joints

Friction stir scribe (FSS) welding as a recent derivative of friction stir welding (FSW) has been successfully used to fabricate a linear joint between automotive Al and steel sheets. It has been established that FSS welding generates a hook-like structure at the bimaterial interface. Beyond the hook-like structure, there is a lack of fundamental understanding on the bond formation mechanism during this newly developed FSS welding process. In this paper, the microstructures and phases at the joint interface of FSS welded Al to ultra-high-strength steel were studied using scanning electron microscopy (SEM) and transmission electron microscopy (TEM). It was found that both mechanical interlocking and interfacial bonding occurred simultaneously during the FSS welding process. Based on SEM observations, a higher diffusion driving force in the advancing side was found compared to the retreating side and the scribe swept zone, and thermally activated diffusion was the primary driving force for the interfacial bond formation in the scribe swept region. The TEM energy-dispersive X-ray spectroscopy (EDXS) revealed that a thin intermetallic compound (IMC) layer was formed through the interface, where the thickness of this layer gradually decreased from the advancing side to the retreating side owing to different material plastic deformation and heat generations. In addition, the diffraction pattern (or one-dimensional fast Fourier transform (FFT) pattern) revealed that the IMC layer was composed of Fe_2Al_5 or Fe_4Al_{13} with a Fe/Al solid solution depending on the weld regions. [DOI: 10.1115/1.4040873]

Keywords: friction stir scribe welding, interfacial layer, interlocking, intermetallic compound

1 Introduction

As the global automotive industry continues its stride in improving fuel efficiency by reducing vehicle weight, more and more aluminum alloys are being used due to their low density, good corrosion resistance, and high recycling potential [1]. However, compared to conventional steels, aluminum alloys have lower strength and formability. Thus, a multimaterial hybrid structure is typically preferred to achieve the desired product performance, demanding the development of reliable dissimilar material joining techniques [2]. Conventional fusion welding of Al to steel is problematic due to their vast differences in melting points, low solid solubility of Fe in Al, and the formation of significant amount of brittle Fe/Al intermetallic compound (IMC) [3]. Friction stir welding (FSW), a solid-state joining technique invented by The Welding Institute (TWI) in 1991 [4], overcomes the issues associated with fusion welding processes owing to the limited heat generation. Recently, significant research has been successfully conducted to investigate the friction stir welded Al to steel joints in the areas of interfacial microstructure characterization [5,6], effects of welding parameters on bond formation [7–11] and mechanical properties [12,13], and numerical process modeling [14–16]. However, it was reported that the metallurgical immiscibility of Al to steel greatly complicates the joint performance since a number of different IMCs could be formed, including FeAl, $FeAl_2$, Fe_2Al_5, and Fe_4Al_{13} [17].

Friction stir scribe (FSS) welding, a recent derivative of FSW invented and developed at the Pacific Northwest National Laboratory, has enabled joining of materials with vastly different melting points by simultaneously producing a mechanical interlock (the hook-like structure) as well as the interfacial bonding at the bimaterial interface with a modified FSW tool [18]. In addition to the typical FSW tool, the FSS tool consists of a cutting tool (scribe cutter) attached at the tip of the FSW pin. A hole is drilled offset from the axis of rotation at the pin tip, and a scribe cutter made from a hard cutting tool material (e.g., WC-Co) is press-fitted into the hole. During the FSS welding process, the conventional FSW tool components (i.e., shoulder and pin) plastically deform the top

[1]Corresponding authors.

Manuscript received January 29, 2018; final manuscript received July 10, 2018; published online August 3, 2018. Assoc. Editor: Wayne Cai.

sheet, and the scribe cutter cuts into the bottom sheet resulting in bonding between the two dissimilar materials. Different from the conventional FSW of dissimilar materials, the shoulder and pin in FSS do not generate bulk plastic deformation of the higher melting temperature material, and bonding can be formed at a temperature below the melting point of the lower melting temperature material. Recently, a few studies have been reported on FSS joints for different material combinations, such as Al to polymer [19], Al to carbon fiber reinforced polyamide [20], and Al to steel [21,22]. Most studies focus on the continuous mechanical interlock formed at the joint interface, i.e., the hook-like structure, while there is a lack of fundamental understanding on the bond formation mechanism at the bimaterial interface of Al and Fe from an interfacial bond formation perspective.

Wang et al. [22] found an Al-Fe intermetallic region on the fracture surface of the steel side in FSS welded Al to galvanized steel joints, indicating that in addition to the mechanical interlock, interfacial bonding also occurred during the welding process. In this paper, the interfacial microstructure of a typical FSS welded Al to ultra-high-strength steel joint is investigated to analyze the interfacial bond formation mechanism. Different IMC bond thicknesses and compositions are found in the advancing and retreating sides, indicating of different diffusion driving force and intrinsic interfacial strength. Since the overall joint mechanical strength depends on the interfacial morphology of the hook-like structure as well as the interfacial bond thickness and intrinsic strength, the current work paves an experimental foundation in predicting and optimizing the FSS welding parameters for dissimilar FSS joint strength. The Al and steel pair can be considered as a representative dissimilar material combination for the FSS welding owing to their vast difference in physical and mechanical properties. The remainder of the paper is organized as follows: Sec. 2 describes the used materials and experimental procedure; Sec. 3 presents the characterized interfacial microstructures in different weld regions using scanning electron microscopy (SEM) and transmission electron microscopy (TEM); Sec. 4 contains the discussions; and Sec. 5 concludes this paper.

2 Materials and Experimental Procedures

2.1 Materials. A representative FSS welded Al to steel joint made between a 1.1 mm thick Surfalex 6 s Al alloy sheet and a 2.0 mm thick hot stamping ultra-high-strength steel (UHSS, Usibor^{R} 1500) sheet was investigated, and Tables 1 and 2 list their chemical composition, respectively. Al-Si coating layer present in the as-received UHSS sheet was grinded off to simplify the interface characterization.

2.2 Experimental Procedures

2.2.1 Friction Stir Scribe Welding Process. A lap configuration was conducted in this study, where a Surfalex 6 s Al alloy sheet (300 mm × 100 mm) was overlapped on the top of a similar size surface grounded UHSS sheet with the overlapped area of 300 mm × 40 mm. The FSS tool shown in Fig. 1 was made from a heat-treated H13 tool steel, while the inserted scribe was made of an M42 cobalt drill bit blank. The FSS tool consisted of a left-handed scrolled shoulder with 3 flat tapered pins. The shoulder was 12.7 mm in diameter, while the maximum pin diameter was 4.2 mm. The effective pin length was 1.0 mm. The scribe diameter was 1.2 mm, while its effective length was 0.32 mm. The scribe was 1.1 mm offset from the axis of rotation. The joint was made at a 0.4 m/min linear welding speed with the rotational speed of 1600 rpm and the commanded plunge depth of 0.85 mm.

Table 1 Chemical composition of as-received Surfalex 6 s Al alloy (Weight %)

Si	Mg	Fe	Cu	Mn	Cr	Zn	Ti	Ni	Al
1.0–1.5	0.3–0.6	<0.3	<0.2	<0.2	<0.1	<0.1	<0.1	0.1	Balance

Table 2 Chemical composition of as-received UHSS (Weight %)

C	Mn	Si	B	Fe
<0.25	<1.4	<0.4	<0.005	Balance

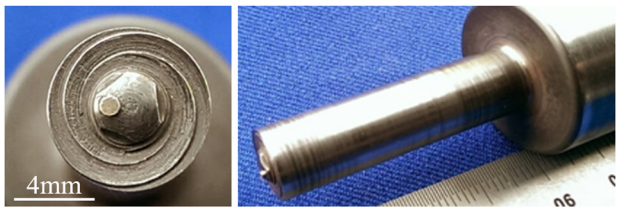

Fig. 1 Friction stir scribe tool geometry

2.2.2 Interfacial Microstructure Characterization. To unveil the characteristics of the joint interfacial microstructures in detail, the cross-sectional microstructure was examined with FEI Nova Nano SEM 630 FESEM at first, where the SEM specimens were cut from the FSS joint perpendicular to the welding direction with a low-speed precision diamond saw followed by a standard metallographic sample preparation process. Based on SEM results, four typical site positions then were selected for TEM observation, where the TEM specimens were cut and extracted using focused ion beam (FIB). Talos F200X operating at 200 kV was used to characterize the microstructure in detail, where the resolution of high angle annular dark field in the scanning transmission electron microscopy (STEM) is down to 0.16 nm. Both TEM and high-resolution transmission electron microscopy images were used to investigate the interfacial phases, where energy-dispersive X-ray spectroscopy (EDXS) in STEM, diffraction pattern, and one-dimensional fast Fourier transform (FFT) pattern were applied to confirm these phases.

3 Results

In this section, the interfacial microstructures of a representative FSS welded Al to steel joint are presented, where the microstructural comparison between the advancing and retreating sides is included.

3.1 Overview of Joint Cross-Sectional Microstructure Based on Scanning Electron Microscopy. Figure 2(*a*) presents a typical joint macrostructure at the interface. It can be seen that both the advancing and retreating sides have a significant interlocking hook (marked as "A" and "B"), while the hook features are different. It is found that the hook in the advancing side was pushed downward (Fig. 2(*b*)) and that in the retreating side was stirred up and flared into the Al sheet (Fig. 2(*c*)). It is noticed that the hooks also have small voids and cracks at the bimaterial interface. This phenomenon indicates that the heat generation close to the hooks was not sufficient to stir the material thoroughly under this welding condition. Between the two hooks, a flat and clean Al-Fe interface is shown in Fig. 2(*a*) within the swept zone, defined by the radial position of the scribe. Also, some stray steel fragments are found embedded in the Al nugget area caused by the shoulder rotation (Fig. 2(*a*)).

For conventional friction stir welded Al to steel joints, IMC is commonly observed [5,7,8]. To understand interface characteristics including existence and nature of IMC at the joint interface generated during the FSS welding process, four typical weld positions were selected for EDXS line scanning and TEM observation

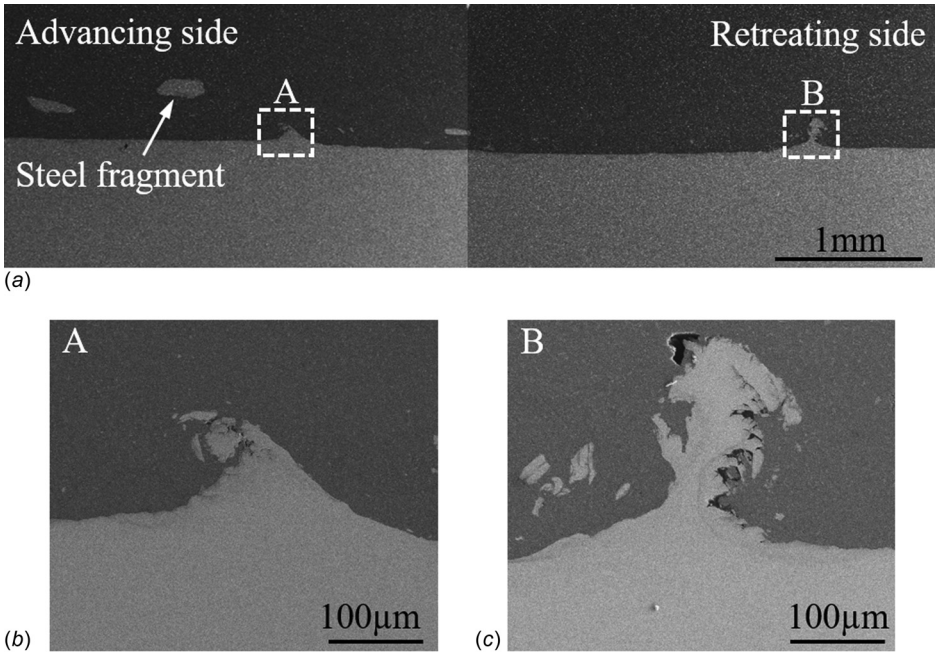

Fig. 2 (*a*) Cross-sectional macrostructure of the FSS welded joint, (*b*) magnified microstructure of the hook in the advancing side, and (*c*) magnified microstructure of the hook in the retreating side

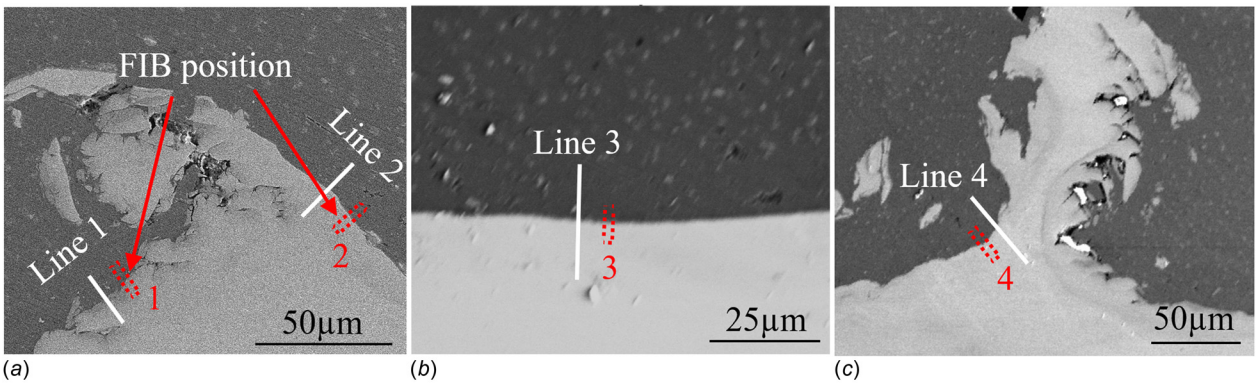

Fig. 3 Selected line scanning and FIB positions (dashed rectangles) at (*a*) the hook in the advancing side, (*b*) middle of the scribe swept zone, and (*c*) the hook in the retreating side

to quantify the chemical composition at the interface, i.e., (1) outside the hook in the advancing side (position 1), (2) inside the hook in the advancing side (position 2), (3) middle of the scribe swept zone (position 3), and (4) inside the hook in the retreating side (position 4). From the comparison of position 1 and the other positions, it is possible to determine the microstructure difference between the scribe swept zone and its adjacent zones. The results at positions 2, 3, and 4 can reveal the bond formation mechanisms and the bonded layer thickness variation in different regions.

Figure 3 illustrates the selected EDXS line scanning and FIB positions, where a TEM sample was cut and extracted from each position next to the line scanning location, as highlighted in the dashed rectangle. Figure 4 presents the corresponding EDXS line scanning results at these four positions. Diffusion layers with various thicknesses are observed at the interface, ranging from 7 μm (along line 1), 6 μm (along line 2), 4 μm (along line 4), to 3.5 μm (along line 3). These observations indicate the higher diffusion driving force in the advancing side than the retreating side and the swept zone, leading to possible differences in the intrinsic bond strength at different locations along the interface. In addition, asymmetrical diffusion profiles are observed for Al and Fe in line 1, line 2, and line 4, indicating different diffusion length, and therefore, different solid state diffusion driving forces exist for the Al and Fe sides at these locations. Although line 1 is located outside the scribe swept zone, compared to the scribe swept zone, more heat and pressure could be transferred from the friction between the conventional tool components (i.e., shoulder and pin) and Al sheet in addition to the scribe effect. Since the hook at this location is the result of the extrusion and pile up of the cut and displaced Fe material from the scribe swept region, solid state diffusion of Al into Fe could be enhanced by the dislocations in the extruded hook, resulting in a thicker diffusion layer at the Fe side of the interface. Different from the other three positions, the line scanning result in the scribe swept zone (i.e., line 3) shows that there is no Al element in Fe side beyond the determined diffusion layer and vice versa, there is no Fe element in Al beyond the diffusion layer. The smooth and symmetrical elemental profile across the interface in line 3 implies that thermally activated diffusion is the primary driving force for the interfacial bond formation in this region. Noted that no significant IMC layer is observed from these line scanning

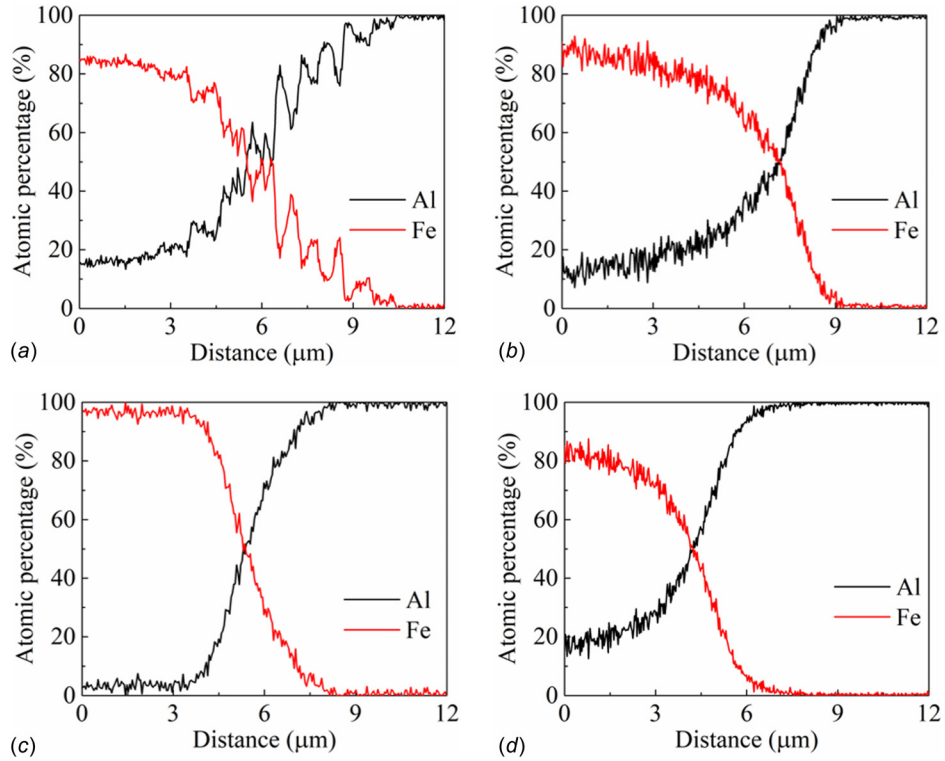

Fig. 4 Line scanning results (*a*) outside the hook in the advancing side (line 1), (*b*) inside the hook in the advancing side (line 2), (*c*) middle of scribe swept zone (line 3), and (*d*) inside the hook in the retreating side (line 4)

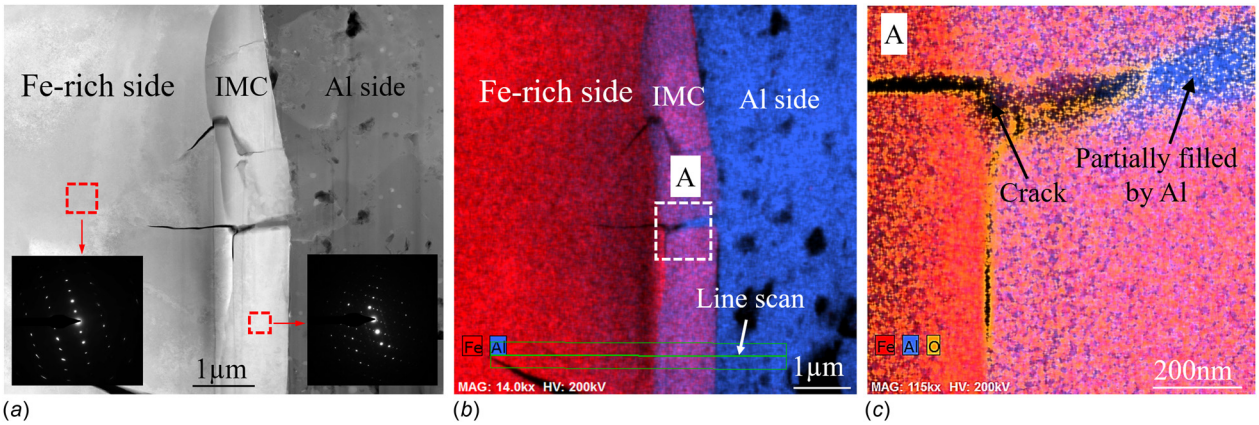

Fig. 5 (*a*) Back scattered electron image of the interfacial microstructure outside the hook in the advancing side (i.e., position 1), (*b*) EDXS map scanning results at this position, and (*c*) high-magnification map scanning results of a crack

results. To confirm these observations, the interfacial microstructures and their chemical compositions are examined using TEM, as presented in the following section.

3.2 Interfacial Microstructure Characterization With Transmission Electron Microscopy. In this section, the microstructure analysis based on TEM observations is presented including interfacial microstructures and chemical compositions. Also, the microstructure variation at different positions is illustrated to help understand the interfacial bond formation during the FSS welding process.

3.2.1 Interfacial Microstructures of the Hook in the Advancing Side (Positions 1 and 2). Figure 5 presents the interfacial microstructure outside the hook in the advancing side (i.e., position 1). The back scattered electron image (Fig. 5(*a*)) shows a thin IMC layer with the thickness of ~1 μm and without clear grain boundary, indicating that its grain size should be larger than 1 μm. Because the thickness of this IMC layer is so small, low magnification SEM based line scan cannot accurately discern its existence and it also leads to the large scatter of the line scanning results as shown in Fig. 4(*a*). Figure 5(*b*) shows the EDXS map scanning results at this position, which confirms the presence of both Al and Fe elements in the IMC layer. Also, no Fe is observed in the Al side while some Al is found in the Fe side (named as Fe-rich side, a Fe/Al diffusion layer), confirming that the solid solubility of Al in Fe is better than that of Fe in Al [23]. From the diffraction pattern comparison between the IMC layer (right lower corner in Fig. 5(*a*)) and the Fe-rich side (left lower corner in Fig. 5(*a*)), it can be seen that the composed crystals are quite

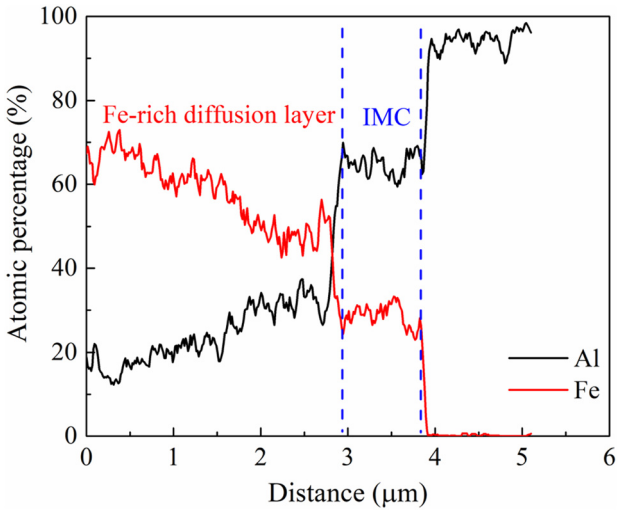

Fig. 6 Energy-dispersive X-ray spectroscopy line scanning results of the sample at position 1

different in these two regions. Moreover, some cracks are found at the interface, which are initiated at the boundary between the Al side and the IMC layer, and propagated across the IMC layer to the Fe-rich side. Figure 5(*c*) presents the high-magnification map scanning results of a crack. The distribution of oxygen element confirms the appearance of this crack, and the partially filled Al implies that the crack generated during the FSS welding process, not after welding or during the TEM sample preparation.

To detect the chemical composition across the interface, a TEM EDXS line scanning was conducted along the line marked in Fig. 5(*b*), and the results are presented in Fig. 6. It can be seen that the interfacial layer consists of two regions, viz., IMC layer and a Fe-rich diffusion layer. The thickness of the IMC layer is ~1 μm confirming the result in Fig. 5(*a*), where the chemical composition is 25% Fe-65% Al (at %). From the Fe–Al binary phase diagram [24] and the observed diffraction pattern of this layer, it is confirmed that Fe_2Al_5 is the intermetallic compound formed. In addition, for the Fe-rich diffusion layer, the Al composition at the initial point of the line scanning is ~18%, indicating that the actual diffusion layer thickness should be larger than the marked area in Fig. 5(*b*).

Figures 7(*a*) and 7(*b*) show high-magnification TEM images of the boundary between the Fe-rich side and the IMC layer, and the IMC layer and the Al side, respectively. Dislocations are observed in the parent metals and the interfacial IMC.

Figures 8(*a*) and 8(*b*) illustrate the interfacial microstructure inside the hook in the advancing side (i.e., position 2) and the magnified IMC layer, respectively. Similar to position 1, a thin IMC layer with the thickness of ~400 nm is observed at the interface and the grain size in this layer is ~150 nm. From the overview of the joint interface (Fig. 8(*a*)), it is found that (1) the Al grains are much larger than the grains in the IMC layer and Fe-rich side; and (2) there are two quite different microstructures in the Fe-rich side, i.e., pure Fe layer (fine Fe grains are observed in this layer) and Fe/Al diffusion layer. It is noted that this pure Fe layer should be attributed to the material tearing and redistribution generated by stirring, not recrystallization, due to the low heat generation during the FSS welding process. Also, the existence of this pure Fe layer is sporadic rather than being consistent. For example, it is not observed in Fig. 4(*b*) due to the slight difference between the line scanning position and the FIB position. From Fig. 8, dislocations and some small Fe particles are observed in the Al side.

Figures 9(*a*) and 9(*b*) show the high-magnification STEM image around the IMC layer and the element distributions across the IMC layer, respectively. Due to limitations of the thin thickness and small grains of the IMC layer, FFT pattern based on high-resolution transmission electron microscopy was captured instead of diffraction pattern to confirm the IMC phase, as presented in Fig. 9(*a*). From the EDXS line scanning results (Fig. 9(*b*)), it is found that the thickness of the IMC layer is ~350 nm, where the variation compared to the one in Fig. 8(*a*) (~400 nm) indicates that the formed IMC layer has a nonuniform thickness. Also, it is noticed that the element distributions in the IMC layer have a gradual change, indicating that this layer includes a Fe/Al solid solution besides the Fe/Al intermetallic compound, which results in the difficulty in determining the Fe/Al ratio to confirm the IMC phase. The chemical composition of this IMC layer is 20~30% Fe-55~62% Al (at %). According to the Fe–Al binary phase diagram [24], three different intermetallic compounds could probably exist in this range, i.e., $FeAl_2$, Fe_2Al_5, and Fe_4Al_{13}. From the observed FFT pattern (upper right corner in Fig. 9(*a*)), it is found that the intermetallic compound in the IMC layer is Fe_2Al_5.

3.2.2 Interfacial Microstructure in the Middle of the Scribe Swept Zone (Position 3). From Fig. 2(*a*), it can be seen that the scribe swept zone (i.e., the area between the hooks in the advancing and retreating sides) constitutes the primary bimaterial interface of the FSS welded joint, and the interfacial bond formation in this region is thus critical for the joint strength in addition to the hooks. Figure 10 presents a typical interfacial microstructure

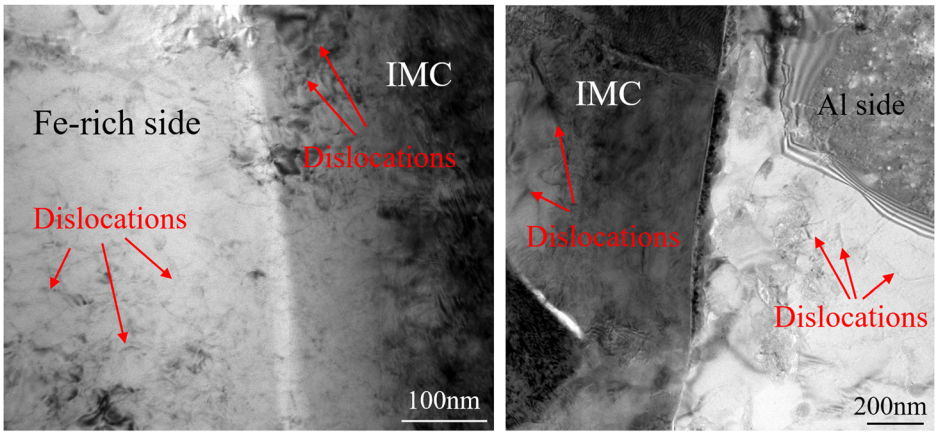

(*a*) (*b*)

Fig. 7 High-magnification TEM images of (*a*) the boundary between Fe-rich side and the IMC layer and (*b*) the boundary between the IMC layer and Al side

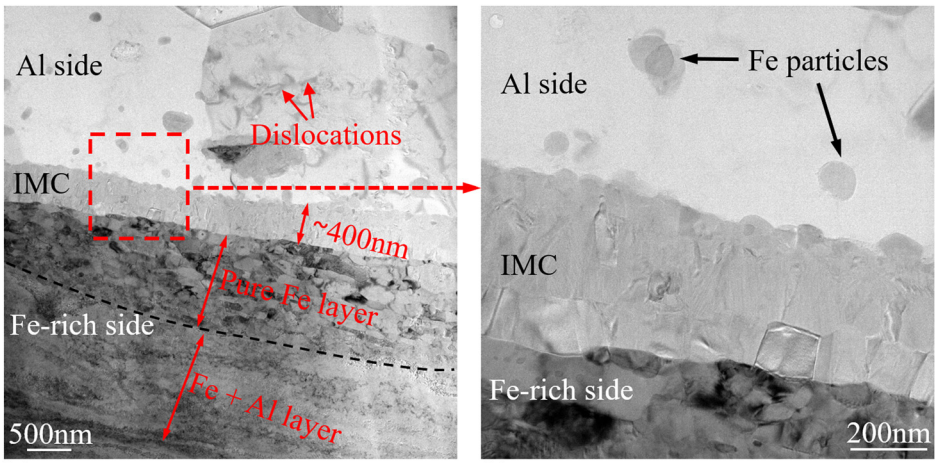

Fig. 8 (*a*) Transmission electron microscopy image of the interfacial microstructure inside the hook in the advancing side (i.e., position 2) and (*b*) high-magnification TEM image of the IMC layer

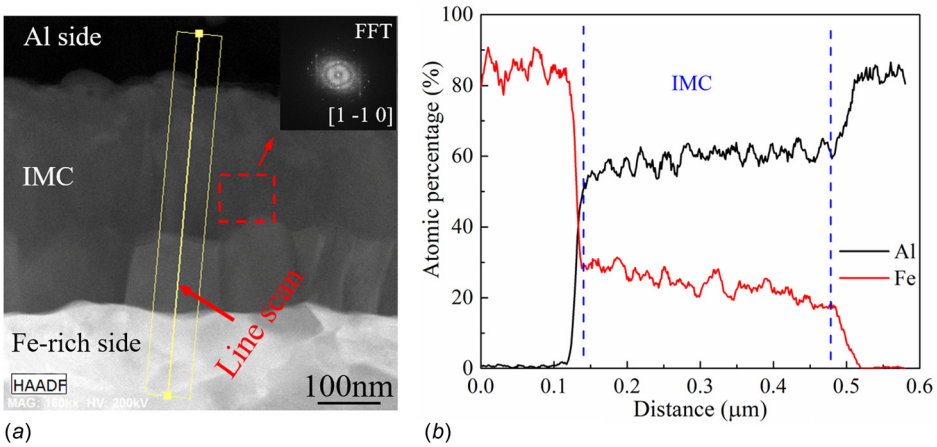

Fig. 9 (*a*) High-magnification STEM image around the IMC layer at position 2 and (*b*) EDXS line scanning results across the IMC layer

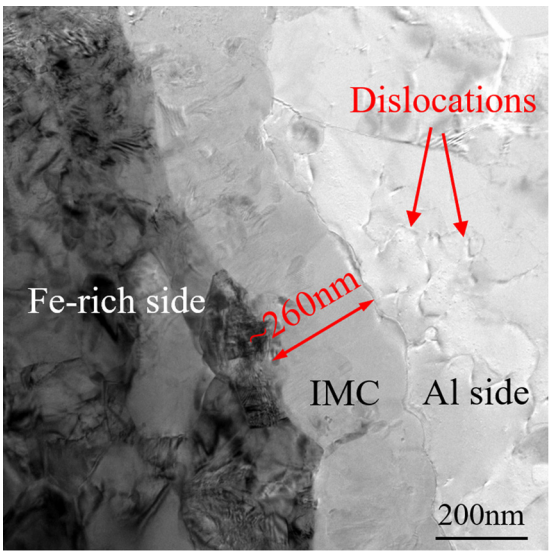

Fig. 10 High-magnification TEM image of the interfacial microstructure in the middle of the scribe swept zone (i.e., position 3)

selected in the middle of the scribe swept zone (i.e., position 3). It is found that similar to positions 1 and 2 (Fig. 8(*b*)), there is a thin IMC layer with the thickness of ~260 nm formed at the interface. Also, dislocations are observed in the Al side and fine Fe grains are found close to the IMC layer.

To identify whether a Fe/Al diffusion layer exists, a low-magnification STEM image at the interface was collected, as shown in Fig. 11(*a*). It is found that the Fe-rich side is composed

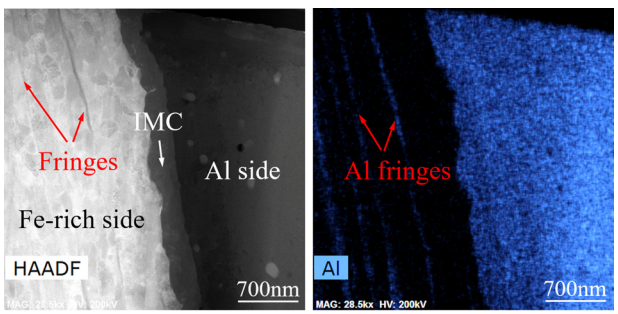

Fig. 11 (*a*) Low-magnification STEM image around the interface at position 3 and (*b*) Al element distribution

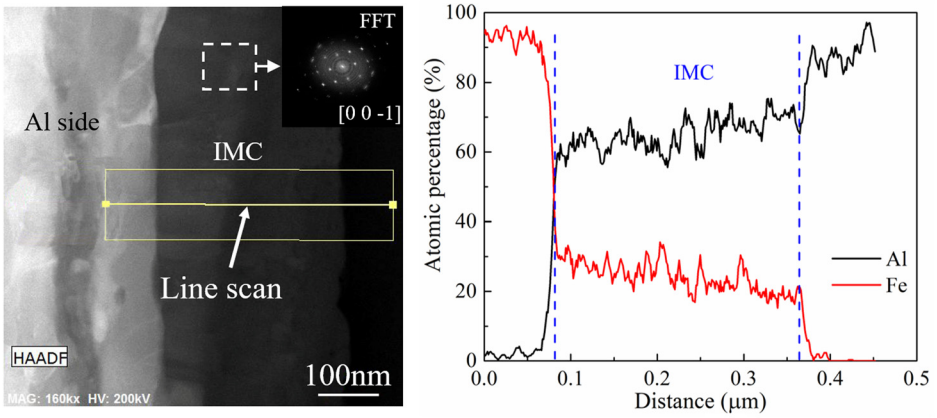

Fig. 12 Energy-dispersive X-ray spectroscopy line scanning results across the IMC layer at position 3

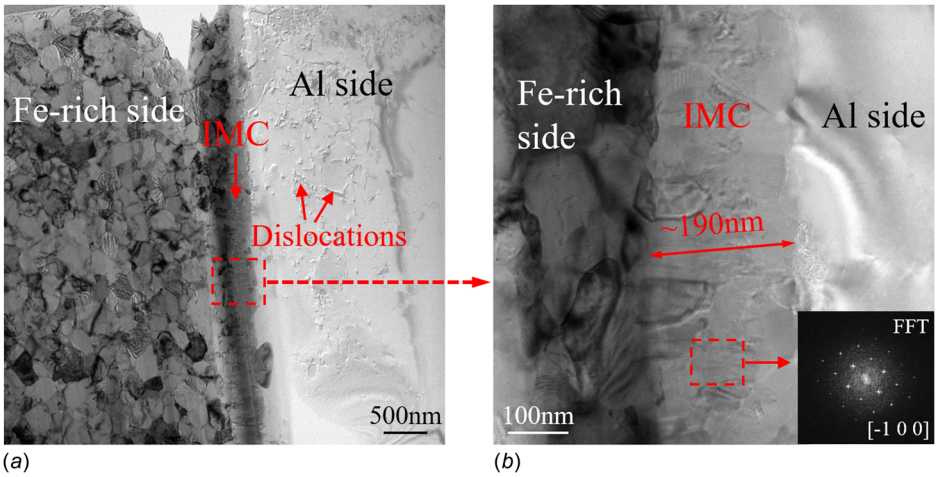

Fig. 13 (*a*) Transmission electron microscopy image of the interfacial microstructure inside the hook in the retreating side (i.e., position 4) and (*b*) high-magnification TEM image of the IMC layer

of Fe grains and several Al fringes appeared between the Fe grains confirmed in Fig. 11(*b*). It is noticed that there is no Fe/Al diffusion layer observed at this position. The appearance of these Al fringes should be introduced during the solid state stirring process. These observations imply that there was no sufficient driving force for Al fringes to diffuse into Fe in the swept zone during the FSS welding process.

Figure 12 presents the EDXS line scanning results across the IMC layer. Similar to the line scanning results at position 2, there is a small gradual change of the element distributions in this IMC layer and the determined FFT pattern (right upper corner in Fig. 12(*a*)) confirms that the Fe_2Al_5 intermetallic compound is formed.

3.2.3 Interfacial Microstructure of the Hook in the Retreating Side (Position 4). Figures 13(*a*) and 13(*b*) present the interfacial microstructures inside the hook in the retreating side (i.e., position 4) and the magnified IMC layer, respectively. A thin IMC layer is also observed at the interface, where the thickness of this IMC layer is ~190 nm. Similar to position 3, the Fe-rich side is composed of fine Fe grains, and dislocations are also observed in the Al side.

To detect the chemical composition of the IMC layer, its STEM and EDXS were conducted, as shown in Fig. 14. From Fig. 14(*a*), it is noted that the white area close to the IMC layer is caused by the nonuniform thickness of the prepared TEM sample, which is much thinner than other regions. However, the reduced thickness should not affect the chemical composition of the IMC layer significantly. Figure 14(*b*) shows the Al element distribution at position 4. It is found that no Al fringes appear in the Fe-rich side, indicating that the material stirring at this position is weaker than the middle of the scribe swept zone. Together with the observed Fe grains in the Fe-rich side, it can be deduced that there is no Fe/Al diffusion layer in the Fe-rich side. Figure 14(*c*) presents the EDXS line scanning results across the IMC layer. Similar to positions 2 and 3, a gradual change of element distributions is found at position 4. However, the determined FFT pattern (right lower corner in Figure 13(*b*)) reveals that the intermetallic compound in the IMC layer is Fe_4Al_{13}.

4 Discussions

Owing to the geometry of the FSS tool and a fairly small scribe engagement into steel, only a small portion of the steel sheet had been cut and plastically deformed by the scribe. Since the total effective length of the scribe was 0.32 mm, while the estimated scribe engagement was ~0.1 mm, the tip of the pin was in close proximity of the location of steel flow, where a thin shear layer (~0.22 mm) existed to separate the steel and pin tip. Thus, the steel transport could be directly influenced by the rotating pin that moved steel from the retreating side to the advancing side, leading to the "pushed-downward" and "stirred-up" features of the hook in the advancing and retreating sides, respectively, as shown in

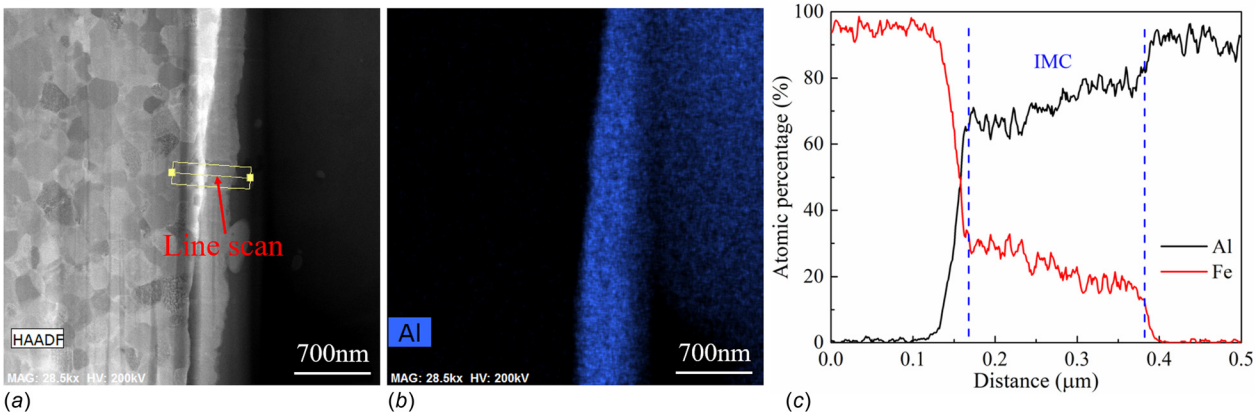

Fig. 14 (*a*) Scanning transmission electron microscopy image around the IMC layer at position 4, (*b*) Al element distribution at the interface, and (*c*) EDXS line scanning results across the IMC layer

Fig. 2. In addition, the steel fragments extruded outside the scribe swept zone in the advancing side confirms the steel transport following the above deduction.

During the FSS welding process, the main heating source to form the interfacial bonding could be divided into two parts, i.e., (1) heat generated from the plastic work dissipation of the steel workpiece by the cutting action of the scribe and (2) heat transferred from plastic dissipation in Al. According to the proposed analytical model by Schmidt et al. [25] based on traditional FSW processes, the tool geometry has a significant effect on the heat generation. In the FSS welding process, a small amount of frictional heat was generated by the scribe due to its small dimension, which results in a weak diffusion between Al and Fe, and thus, some Al fringes rather than a diffusion region in the Fe-rich side are observed in the middle of the scribe swept zone. As stated by Rathod and Kutsuna [26], the generation of IMC at the interface involves two stages, i.e., (1) forming a supersaturated solid solution based on the atoms diffusion across the interface and (2) transforming the supersaturated solid solution into an IMC once its composition reaches to a sufficient level. Owing to the limited heat generation and the low solid solubility of Fe in Al, the thickness of formed IMC layer is small. Also, it is noticed that there is a residual Fe/Al solid solution in the IMC layer, which causes the small gradual change of the element distributions in this layer.

As illustrated in Fig. 2(*a*), some steel was extruded outside the scribe swept zone to form the hooks, and the transferred heat from the tool friction with the Al sheet facilitated the growth of generated IMC. On the other hand, the continuous scribe engagement introduced intense plastic deformation at the interface, and thus, the grains in the IMC layer were significantly refined, as shown in Fig. 8(*b*). Therefore, the IMC layer in the hook outside the scribe swept zone (position 1) has larger grains than those in the scribe swept zone (positions 2, 3, and 4). Based on the microhardness comparisons, welding temperature measurements, and stress/strain rate analysis [27,28], it is widely accepted that the heat generation in the advancing side is higher than that in the retreating side in FSW. Although there was no direct temperature measurement in this study, similar heat generation asymmetry between advancing and retreating sides might be applicable in FSS. Thus, the higher heat generation in the advancing side led to a thicker IMC layer compared to the retreating side and a significant Fe/Al diffusion layer in the Fe-rich side. For instance, the thickness of the IMC layer inside the hook in the advancing side (position 2) is ~400 nm, and that in the retreating side (position 4) is ~190 nm.

In addition, small cracks are observed at the Al/Fe interface in the hook region, which propagated across the IMC layer to the Fe-&rich side, as shown in Fig. 5(*a*). These small cracks at the interface, depending on their locations, might influence the fracture path during strength testing under different fracture modes. However, it is difficult to quantitatively ascertain the influence since failure during lap-shear testing often occurs away from the weld region in Al base metal, depending on sample geometry [20].

5 Conclusions

In this paper, the interfacial bonding mechanism of FSS welded Al to ultra-high-strength steel joints was investigated, where four typical weld positions were selected to determine the microstructure characteristics in different regions. The main conclusions can be summarized as follows:

(1) Both mechanical interlocking and interfacial bonding occurred simultaneously during the FSS welding process. In addition to the generated mechanical interlock hooks, a very thin IMC layer (190 nm~1 μm) was observed at the Al/Fe interface due to the low heat generation and the low solid solubility of Al in Fe.
(2) Because the plastic deformation and heat generation were decreasing from the advancing side to the retreating side, the diffusion driving force in the advancing side was found higher than that in the retreating side and the scribe swept zone, and the thickness of the IMC layer decreased from the advancing side to the retreating side.
(3) According to the EDXS line scanning results and diffraction FFT patterns, it was found that the IMC layer was composed of Fe_2Al_5 or Fe_4Al_{13} with a Fe/Al solid solution depending on the weld regions.

Acknowledgment

The authors also like to acknowledge Fiat Chrysler Automobile, U.S. LLC for providing materials relevant to this work.

Funding Data

- US National Science Foundation Civil, Mechanical and Manufacturing Innovation (Grant Nos. 1363468 and 1651024).
- The Pacific Northwest National Laboratory is operated by the Battelle Memorial Institute for the United States Department of Energy under contract DE-AC06-76 LO1830.
- The U.S. Department of Energy Vehicles Technologies Office (DOE/VTO).

References

[1] Miller, W. S., Zhuang, L., Bottema, J., Wittebrood, A. J., De Smet, P., Haszler, A., and Vieregge, A., 2000, "Recent Development in Aluminium Alloys for the Automotive Industry," Mater. Sci. Eng. A, **280**(1), pp. 37–49.
[2] Martinsen, K., Hu, S. J., and Carlson, B. E., 2015, "Joining of Dissimilar Materials," CIRP Ann., **64**(2), pp. 679–699.
[3] Hansen, M., 1958, "*Constitution of Binary Alloys*," McGraw-Hill Book Company, New York.

[4] Thomas, W. M., Nicholas, E. D., Needham, J. C., Murch, M. G., Temple-Smith, P., and Dawes, C. J., 1991, "Friction Stir Butt Welding," GB Patent No. 9125978.8.
[5] Elrefaey, A., Gouda, M., Takahashi, M., and Ikeuchi, K., 2005, "Characterization of Aluminum/Steel Lap Joint by Friction Stir Welding," J. Mater. Eng. Perform., **14**(1), pp. 10–17.
[6] Zheng, Q., Feng, X., Shen, Y., Huang, G., and Zhao, P., 2016, "Dissimilar Friction Stir Welding of 6061 Al to 316 Stainless Steel Using Zn as a Filler Metal," J. Alloys Compd., **686**, pp. 693–701.
[7] Shen, Z., Chen, Y., Haghshenas, M., and Gerlich, A. P., 2015, "Role of Welding Parameters on Interfacial Bonding in Dissimilar Steel/Aluminum Friction Stir Welds," Eng. Sci. Tech. Int. J., **18**(2), pp. 270–277.
[8] Pourali, M., Abdollah-zadeh, A., Saeid, T., and Kargar, F., 2017, "Influence of Welding Parameters on Intermetallic Compounds Formation in Dissimilar Steel/Aluminum Friction Stir Welds," J. Alloys Compd., **715**, pp. 1–8.
[9] Dehghani, M., Amadeh, A., and Akbari Mousavi, S. A. A., 2013, "Investigations on the Effects of Friction Stir Welding Parameters on Intermetallic and Defect Formation in Joining Aluminum Alloy to Mild Steel," Mater. Des., **49**, pp. 433–441.
[10] Liu, X., Lan, S., and Ni, J., 2014, "Analysis of Process Parameters Effects on Friction Stir Welding of Dissimilar Aluminum Alloy to Advanced High Strength Steel," Mater. Des., **59**, pp. 50–62.
[11] Chen, K., Liu, X., and Ni, J., 2017, "Effects of Process Parameters on Friction Stir Spot Welding of Aluminum Alloy to Advanced High-Strength Steel," ASME J. Manuf. Sci. Eng., **139**(8), p. 081016.
[12] Yazdipour, A., and Heidarzadeh, A., 2016, "Effect of Friction Stir Welding on Microstructure and Mechanical Properties of Dissimilar Al 5083-H321 and 316 L Stainless Steel Alloy Joints," J. Alloys Compd., **680**, pp. 595–603.
[13] Movahedi, M., Kokabi, A. H., Seyed Reihani, S. M., and Najafi, H., 2012, "Effect of Tool Travel and Rotation Speeds on Weld Zone Defects and Joint Strength of Aluminium Steel Lap Joints Made by Friction Stir Welding," Sci. Tech. Weld. Joining, **17**(2), pp. 162–167.
[14] Jedrasiak, P., Shercliff, H. R., Reilly, A., McShane, G. J., Chen, Y. C., Wang, L., Robson, J., and Prangnel, P., 2016, "Thermal Modeling of Al-Al and Al-Steel Friction Stir Spot Welding," J. Mater. Eng. Perform., **25**(9), pp. 4089–4098.
[15] Liu, X., Chen, G., Ni, J., and Feng, Z., 2017, "Computational Fluid Dynamics Modeling on Steady-State Friction Stir Welding of Aluminum Alloy 6061 to TRIP Steel," ASME J. Manuf. Sci. Eng., **139**(5), p. 051004.
[16] Liu, X., Lan, S., and Ni, J., 2015, "Thermal Mechanical Modeling of the Plunge Stage During Friction-Stir Welding of Dissimilar Al 6061 to TRIP 780 Steel," ASME J. Manuf. Sci. Eng., **137**(5), p. 051017.
[17] Sundman, B., Ohnuma, I., Dupin, N., Kattner, U. R., and Fries, S. G., 2009, "An Assessment of the Entire Al-Fe System Including $D0_3$ Ordering," Acta Mater., **57**(10), pp. 2896–2908.
[18] Hovanski, Y., Grant, G. J., Jana, S., and Mattlin, K. F., 2013, "Friction Stir Welding Tool and Process for Welding Dissimilar Materials," U.S. Patent No. 8434661 B2.
[19] Upadhyay, P., Hovanski, Y., Fifield, L. S., Simmons, K. L., 2015, "Friction Stir Lap Welding of Aluminum-Polymer Using Scribe Technology," *Friction Stir Welding and Processing VIII*, R. S. Mishra, M. W. Mahoney, Y. Sato, and Y. Hovanski, eds., Wiley, Hoboken, NJ, pp. 153–160.
[20] Upadhyay, P., Hovanski, Y., Jana, S., and Fifield, L. S., 2017, "Joining Dissimilar Materials Using Friction Stir Scribe Technique," ASME J. Manuf. Sci. Eng., **139**(3), p. 03450.
[21] Curtis, T., Widener, C., West, M., Jasthi, B., Hovanski, Y., Carlson, B., Szymanski, R., Bane, W., 2015, "Friction Stir Scribe Welding of Dissimilar Aluminum to Steel Lap Joints," *Friction Stir Welding and Processing VIII*, R. S. Mishra, M. W. Mahoney, Y. Sato, and Y. Hovanski, eds., Wiley, Hoboken, NJ, pp. 163–169.
[22] Wang, T., Sidhar, H., Mishra, R. S., Hovanski, Y., Upadhyay, P., and Carlson, B. E., 2017, "Friction Stir Scribe Welding Technique for Dissimilar Joining of Aluminium and Galvanized Steel," Sci. Tech. Weld. Joining, **23**(3), pp. 249–255.
[23] Davis, J. R., 2001, *ASM Specialty Handbook: Aluminum and Aluminum Alloys*, ASM International, Material Park, OH, p. 379.
[24] Massalski, T. B., and Okamoto, H., 1990, *Binary Alloy Phase Diagrams*, ASM International, Material Park, OH, p. 147.
[25] Schmidt, H., Hattel, J., and Wert, J., 2004, "An Analytical Model for the Heat Generation in Friction Stir Welding," Modell. Simul. Mater. Sci. Eng., **12**(1), pp. 143–157.
[26] Rathod, M. J., and Kutsuna, M., 2004, "Joining of Aluminum Alloy 5052 and Low-Carbon Steel by Laser Roll Welding," Weld. J., **83**(7–8), pp. 16S–26S.
[27] Wade, M., and Reynolds, A. P., 2010, "Friction Stir Weld Nugget Temperature Asymmetry," Sci. Tech. Weld. Joining, **15**(1), pp. 64–69.
[28] Upadhyay, P., and Reynolds, A. P., 2012, "Effects of Forge Axis Force and Backing Plate Thermal Diffusivity on FSW of AA6056," Mater. Sci. Eng. A, **558**, pp. 394–402.